

Article

Highly Sensitive p + n Metal Oxide Sensor Array for Low-Concentration Gas Detection

Jianghua Luo ¹, Yishan Jiang ^{1,*}, Feng Xiao ¹, Xin Zhao ¹ and Zheng Xie ²

¹ Navy Submarine Academy, Qingdao 266199, China; 13061405315@sina.cn (J.L.); qdxuwx@126.com (F.X.); 13156239571@163.com (X.Z.)

² State Key Laboratory of Chemical Resource Engineering, Beijing University of Chemical Technology, North Third Ring Road 15, Beijing 100029, China; zheng163xie@163.com

* Correspondence: jys130@126.com

Received: 5 July 2018; Accepted: 7 August 2018; Published: 17 August 2018



Abstract: Nowadays, despite the easy fabrication and low cost of metal oxide gas sensors, it is still challenging for them to detect gases at low concentrations. In this study, resistance-matched p-type Cu₂O and n-type Ga-doped ZnO, as well as p-type CdO/LaFeO₃ and n-type CdO/Sn-doped ZnO sensors were prepared and integrated into p + n sensor arrays to enhance their gas-sensing performance. The materials were characterized by scanning electron microscopy, transmittance electron microscopy, and X-ray diffractometry, and gas-sensing properties were measured using ethanol and acetone as probes. The results showed that compared with individual gas sensors, the response of the sensor array was greatly enhanced and similar to the gas response product of the p- and n-type gas sensors. Specifically, the highly sensitive CdO/LaFeO₃ and CdO/Sn-ZnO sensor array had a high response of 21 to 1 ppm ethanol and 14 to 1 ppm acetone, with detection limits of <0.1 ppm. The results show the effect of sensor array integration by matching the two sensor resistances, facilitating the detection of gas at a low concentration.

Keywords: metal oxide semiconductor; p + n sensor array; low concentration; ethanol and acetone sensing

1. Introduction

Nowadays, due to their easy fabrication and low cost, metal oxide (MOX) gas sensors have been widely investigated to be applied in inflammable gas alarms and toxic gas detection [1–4]. Although they are now extensively used to detect the leakage of inflammable gases such as H₂, CH₄, etc. in the range of 0.1–5%, their detection of low-concentration gases, such as air pollutants (e.g., formaldehyde in indoor air) and breath organics (e.g., acetone as a sensor for diabetes) at the ppb–ppm level, is still technologically challenging [5–11].

One major strategy to solve this problem is the development of highly sensitive MOX materials, such as stoichiometrically and morphologically tuned SnO₂, ZnO, In₂O₃, and WO₃ materials [12–19]. For example, Chen et al. reported that Fe₂O₃/SnO₂ core–shell nanorods had a high response of 20 to 10 ppm ethanol [20], and Zhang et al. synthesized heterostructured ordered ZnO-Fe₃O₄ inverse opal materials for the highly sensitive detection of acetone with a response of 2 to 1 ppm acetone [13]. Meanwhile, there is another strategy to improve the gas response using a sensor array design. Generally, p- and n-type gas-sensing materials have reverse responses to the same gases, that is to say, resistance increases in p-type MOX with reductive gases (e.g., ethanol), while resistance decreases in n-type MOX [21]. Wang et al. firstly designed a p-type (Co₂O₃) and n-type (SnO₂) gas sensor array in order to use the complementary effect of p- and n-type gas sensors [22]. Using this sensor array, a response of ~38 was obtained to 1000 ppm toluene [23], and humidity selectivity can also be achieved by

a two-sensor array [5]. However, a limitation is that highly sensitive p-type MOX materials are usually scarce compared with n-type materials.

In this study, we synthesized novel p-type Cu_2O and LaFeO_3 materials for the integration of a p + n sensor array, combining them with typical n-type doped ZnO materials. The results showed that the response of the sensor array was similar to the response product of the p- and n-type gas sensors. Specifically, the $\text{CdO}/\text{LaFeO}_3$ and $\text{CdO}/\text{Sn-doped ZnO}$ sensor array had high responses of 21 and 14 to 1 ppm ethanol and acetone, respectively, with a low detection limit of <0.1 ppm. The synthesis of highly sensitive p-type materials and the resistance matching of the p- and n-type sensors are found to be the main aspects of sensor array designs.

2. Experimental Method

Cu_2O , Ga-doped ZnO, and Sn-doped ZnO were synthesized using the precipitation method, and the LaFeO_3 material was obtained by sol-gel self-ignition [24–27]. Typically, Cu_2O is produced by the reduction of Cu (II) with glucose. Firstly, 1 mL of CuSO_4 solution (0.68 M) was diluted in 17 mL of water, and 1 mL of sodium citrate (0.74 M) and 1 mL of Na_2CO_3 were then added to make a blue solution. This was then kept at 80 °C in a water bath and 1 mL of 1.4 M glucose was added. After reacting for 2 h, the precipitate was separated by centrifuge and rinsed with water and ethanol to obtain the Cu_2O product. Ga- and Sn-doped ZnO were obtained by co-precipitation. Firstly, 50 mL of ZnSO_4 and 2.2 mol % GaCl_3 (or SnCl_2) were added to 100 mL of NH_4HCO_3 , and the precipitation was rinsed and calcined at 500 °C for 2 h to obtain the product. For LaFeO_3 , $\text{La}(\text{NO}_3)_3$, $\text{Fe}(\text{NO}_3)_3$, and citric acid were dissolved in water. Ammonia was added to the solution to maintain the pH at 6–7 and the solution turned into a sol in a 75 °C water bath. The sol was then dried in an oven at 130 °C to form a dry gel, which was then ignited and annealed at 600 °C for 2 h to obtain the product. CdO was decorated onto the materials by immersing the powders in a $\text{Cd}(\text{NO}_3)_2$ solution, which was then dried and calcined at 500 °C for 2 h.

The morphology and energy dispersive spectra (EDS) were observed using a scanning electron microscope (SEM, JEOL JSM-6700F, Japan, 15 kV, 10 μA) and a transmittance electron microscope (TEM, JEOL JEM-2010F, Tokyo, Japan, 200 kV, 100 μA). The crystal phase was identified by X-ray diffraction (XRD) on a Panalytical X-ray diffractometer with $\text{CuK}\alpha$ radiation of 0.154 nm (40 kV, 40 mA) and a high-resolution TEM (HRTEM). Gas-sensing performance was measured in a homemade gas sensor test instrument [28] as shown in Figure 1a. The sensing materials were drop-coated on Al_2O_3 substrates, which had two Pt wires attached on both ends by Ag paste. The two sensors were placed in a two-zone tube furnace to achieve the working temperature, and the gases to be detected were introduced into the tube furnace (diameter 40 mm) by a mass flow controller. The gas concentration of 0.1–1 ppm was controlled by diluting 5 ppm standard ethanol and acetone gases with synthetic air. Additionally, 1–5 ppm gas was obtained by diluting 50 ppm standard gas with synthetic gas. For example, 0.1 ppm ethanol was obtained by mixing 10 sccm 5 ppm ethanol gas with 490 sccm synthetic air. The voltage bias was 5 V, and the voltage (V_{OUT}) on the load resistance was recorded for the n-type MOX sensor, while the voltage (V_{OUT}) on the p-type MOX sensor was recorded for the p-type sensor and p + n sensor array as shown in Figure 1a–c. The response was defined as the resistance ratio of R_a/R_g for the n-type sensor and R_g/R_a for the p-type sensor to the reductive gases, where R_a and R_g are the sensor resistances in air and in detected gases, respectively, which are calculated from the measured voltage as follows: R_a and $R_g = R(5/V_{\text{OUT}} - 1)$ [29].

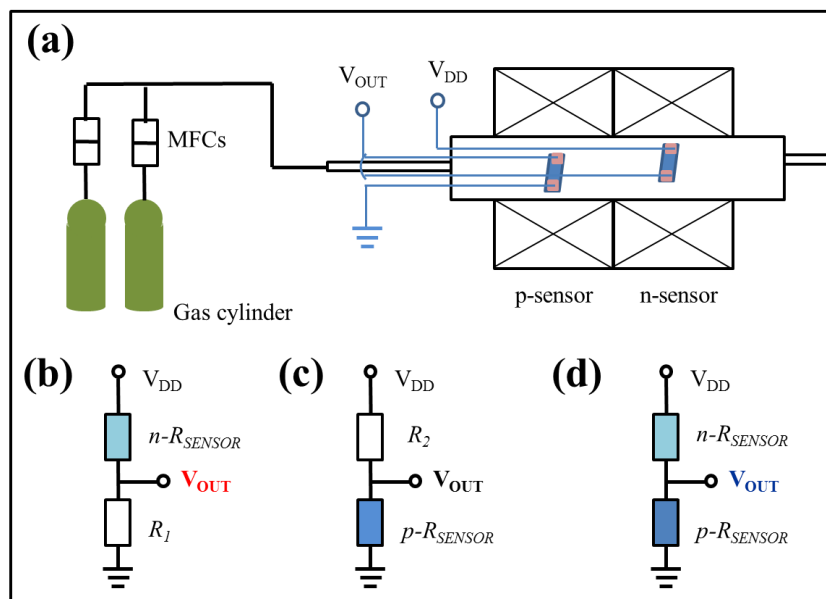


Figure 1. Schematics of the (a) gas sensor measurement system, (b) n-sensor, (c) p-sensor, and (d) p + n sensor array circuits.

3. Results and Discussion

The p-type Cu_2O material was typically cubes, as shown in the SEM and TEM images in Figure 2a,b, with an edge length of $\sim 0.5 \mu\text{m}$. The HRTEM image in Figure 2b shows the typical (111) plane spacing of 0.246 nm in the cubic phase. The cubic phase was also identified by the XRD pattern in Figure 2c in good accordance with the standard card Powder Diffraction File (PDF) 00-005-0667. The cubic shape was attributed to the relatively low surface energy of the (100) surfaces as compared with others such as (111). This is in good agreement with the literature reporting that if surfactant (e.g., polyvinyl pyrrolidone) is used to stabilize the (111) plane, then octahedral shaped Cu_2O would be obtained, exposing (111) planes, and if there is no surfactant, cubes would be produced, exposing (100) planes [30–32].

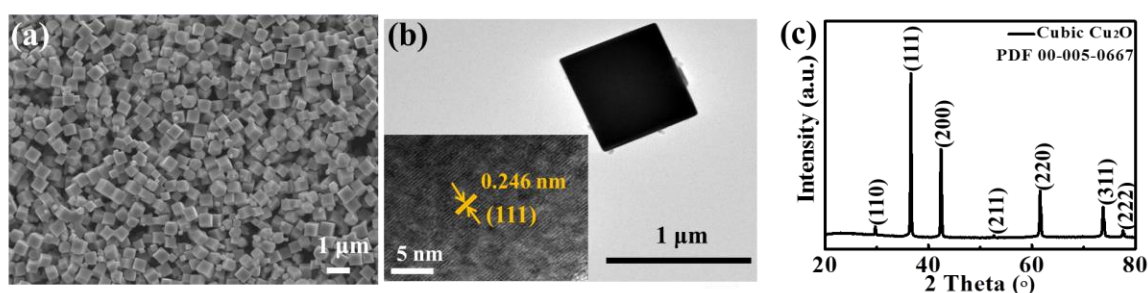


Figure 2. Characterization of p-type Cu_2O sensing material: (a) SEM, (b) TEM and HRTEM (inset), and (c) XRD pattern.

Subsequently, another typical n-type sensing material, 2.2 mol % Ga-doped ZnO, was prepared and characterized as shown in Figure 3. As shown in the SEM image in Figure 3a, the Ga-ZnO nanoparticles had a diameter of 20–50 nm, and Ga was identified by the EDS spectrum as shown in the inset. The plane spacings in the HRTEM image and the fast Fourier transmission (FFT) in Figure 3b correspond well with the lattice of ZnO. There was no extra Ga_2O_3 phase identified by the XRD pattern besides the hexagonal ZnO phase (PDF 01-076-0704), as shown in Figure 3c, because the Ga atoms are doped into the ZnO lattice in order to tune the resistance.

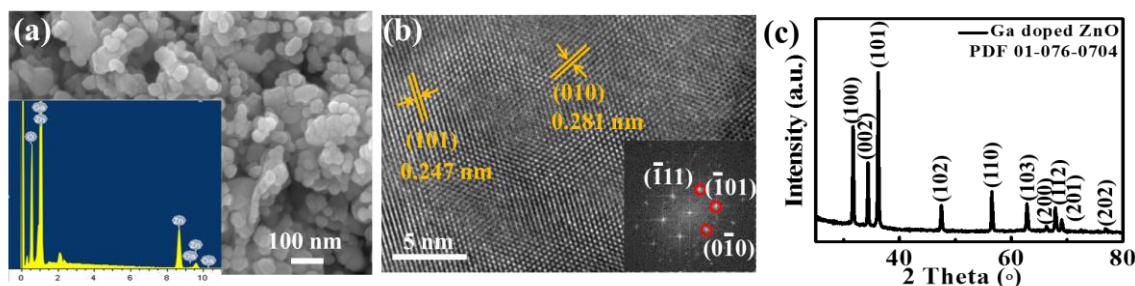


Figure 3. Characterization of n-type Ga-doped ZnO sensing material: (a) SEM and energy dispersive spectrum (EDS) (inset); (b) HRTEM and fast Fourier transmission (FFT) (inset); (c) XRD pattern.

The ethanol-sensing performance of Cu_2O and Ga-ZnO were measured and calculated as shown in Figure 4a,b. Figure 4a shows that Cu_2O had an optimal working temperature of 200 °C with a response of 1.3 to 5 ppm ethanol. This low working temperature ensures the high stability of the Cu_2O sensor, as it is thermally oxidized into CuO at temperatures of >250 °C as reported in the literature [24,33]. Moreover, the resistance increasing in ethanol ($R_g/R_a > 1$) indicates the p-type conductivity of the Cu_2O material. On the other side, Ga-ZnO showed a typical n-type sensing performance ($R_a/R_g > 1$ in ethanol) as shown in Figure 4b, with an optimal working temperature of 400 °C (response of 5.7 to 5 ppm ethanol). Subsequently, the p-type Cu_2O and n-type Ga-ZnO sensors were integrated into a sensor array as shown in Figure 1c to measure their ethanol-sensing performance. As shown in Figure 4c, the dynamic response curves clearly show the enhanced response of the sensor array compared with the single sensors, with little influence on the response/recovery times. The response/recovery times were in the scale of several minutes, as the inlet gas needs a relatively long time of several minutes to achieve equilibrium in the large-volume quartz tube. Response versus ethanol concentration is plotted in Figure 4d, where a response of about 8.5 is obtained, similar to the response product of the Cu_2O and Ga-ZnO sensors ($1.3 \times 5.7 = 7.4$).

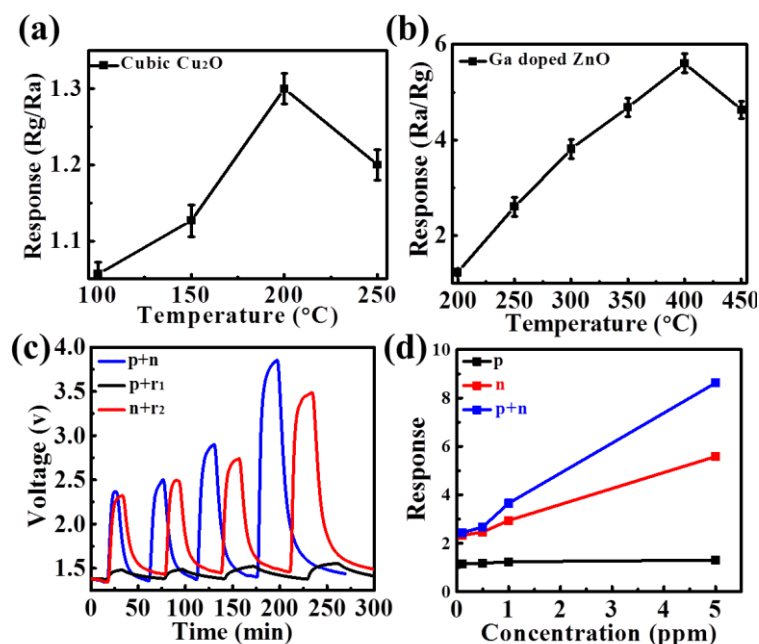


Figure 4. (a) Response of Cu_2O p-sensor to 5 ppm ethanol at different working temperatures; (b) response of Ga-ZnO n-sensor to 5 ppm ethanol at different working temperatures; (c) responses of Ga-ZnO n-sensor, Cu_2O p-sensor, and p + n sensor array to 5 ppm ethanol; and (d) relationship of Ga-ZnO n-sensor, Cu_2O p-sensor, and p + n sensor array responses with ethanol concentrations.

It should be noted that although the sensor array had an enhanced response, this enhancement was limited by the relatively low response of the p-type Cu_2O sensor. Therefore, we prepared another p-type sensing material, perovskite LaFeO_3 , which is activated by CdO decoration to enhance the response [21,34,35]. As shown in the SEM image in Figure 5a, the CdO/ LaFeO_3 material was composed of nanoparticles with a diameter of ~ 50 nm, with typical La, Fe, O, and Cd identified by the EDS spectrum in the inset. The HRTEM image and corresponding FFT in Figure 5b clearly show the typical perovskite (220) and (102) lattice spacings of LaFeO_3 . Furthermore, the XRD pattern shows the perovskite structure of LaFeO_3 with no CdO peaks observed due to the relatively low dosage (5 mol %).

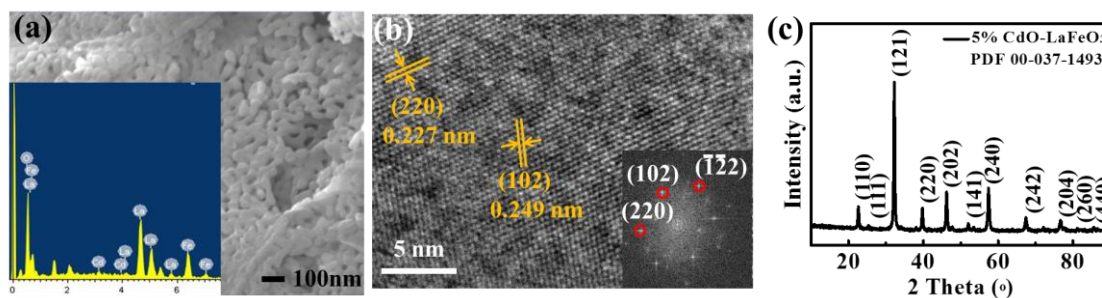


Figure 5. Characterizations of CdO-activated p-type LaFeO_3 : (a) SEM image and EDS spectrum (inset); (b) HRTEM and FFT (inset) and (c) XRD pattern.

However, this kind of LaFeO_3 material has a relatively large resistance in the order of 10^9 ohm, much higher than that of Cu_2O and Ga-ZnO (10^6 ohm), making it difficult to integrate the sensor array with Ga-ZnO. Therefore, another kind of n-type material, Sn-doped ZnO, was prepared and activated by 10 mol % CdO decoration [35] to enhance the sensitivity. As shown in Figure 6a, the CdO/Sn-ZnO material was also composed of nanoparticles with a diameter of 10–50 nm, and Cd, Sn, Zn, and O were all identified by the EDS spectrum in the inset. The lattice spacings in the HRTEM image in Figure 6b correspond well with the ZnO lattice. Importantly, the XRD pattern in Figure 6c indicates the hexagonal phase of the ZnO material, with extra CdO-related weak peaks identified. This is due to the relatively higher dosage of CdO (10 mol %) than that in CdO/ LaFeO_3 . It is noticed that both materials, CdO-activated LaFeO_3 and Sn-ZnO, have a porous structure as shown in Figures 5a and 6a, which favors the gas diffusion and reaction and would thus enhance the gas response.

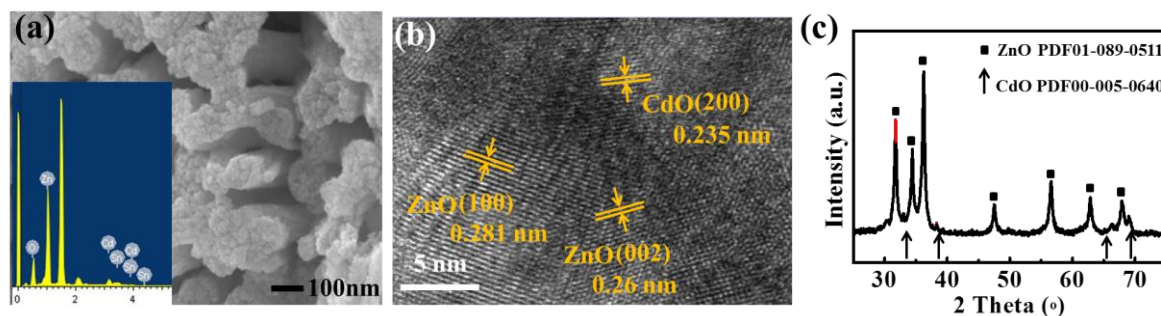


Figure 6. Characterizations of CdO-activated n-type Sn-doped ZnO: (a) SEM image and EDS spectrum (inset); (b) HRTEM and FFT (inset); and (c) XRD pattern.

Subsequently, these two sensors were integrated into a sensor array and the responses to typical ethanol and acetone gases are shown in Figure 7. The individual sensor responses of p-type CdO/ LaFeO_3 and n-type CdO/Sn-ZnO to 1 ppm ethanol were 8.5 and 3.5 at working temperatures of 200 and 300 °C, respectively, as shown in Figure 7a. The sensor array had an enhanced response of 21 to 1 ppm ethanol, similar to the product of 8.5×3.5 as shown in Figure 7b. The detection limit

can be as low as 0.1 ppm for the sensor array with an obvious response of 4, showing the advantage of the sensor array in the detection of low-concentration gases. Normally, a response of 2–3 can be estimated as the detection limit; thus, the sensor array had a detection limit of <0.1 ppm. Furthermore, the responses to 1 ppm acetone were measured as shown in Figure 7c, where responses of 5.1 and 3.5 are observed for the CdO/LaFeO₃ and CdO/Sn-ZnO sensors at optimal working temperatures of 200 and 300 °C, respectively. Thus, the sensor array had an enhanced response of 14 to 1 ppm acetone as shown in Figure 7d, with a low detection limit of <0.1 ppm. These are promising results for the use of this sensor array to detect traces of gas with concentrations at sub-ppm levels.

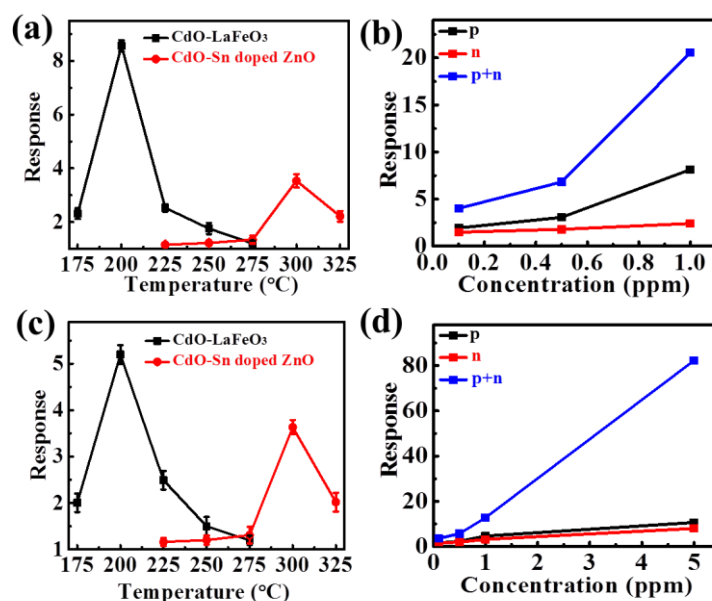


Figure 7. Responses of CdO-activated LaFeO₃ and Sn-ZnO: (a,b) relationships of ethanol response with working temperature and concentration, respectively; (c,d) relationships of acetone response with working temperature and concentration, respectively.

However, there is an issue with the complex resistance matching of the sensors. As mentioned above, sensors with a respective resistance of 10^9 and 10^6 ohm cannot be integrated into an effective sensor array because there would not be any significant voltage change in the circuit, as depicted in Figure 1c. For example, the voltage output on the 10^6 -ohm sensor would be 0.005 V. A response of 10 would give an output voltage of only 0.05 V, which is too low to be effectively measured by the output circuits. The sensor resistances are plotted in Figure 8 to further illustrate this resistance matching problem. P-type Cu₂O has a relatively low resistance, and that of n-type ZnO is orders of magnitude higher. Therefore, Ga was adopted as the effective dopant to reduce the resistance of n-type ZnO to a similar level to that of Cu₂O. On the other hand, p-type LaFeO₃ has a similar resistance to that of ZnO; thus, they can compose the sensor array. Additionally, the Sn dopant and the CdO activator were only used for enhancing the sensitivity of the material rather than tailoring the resistance. Therefore, all these results indicate the effective response enhancement of the well-tuned p + n sensor array for low-concentration gas detection.

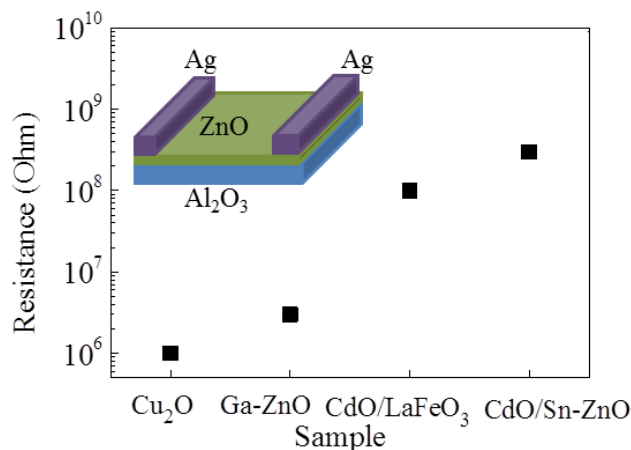


Figure 8. Gas sensor resistance selection rules for effective p + n sensor arrays.

4. Conclusions

P-type Cu₂O and CdO/LaFeO₃ as well as n-type Ga-doped ZnO and CdO/Sn-doped ZnO sensing materials were prepared, and effective p + n gas sensor arrays were designed and fabricated for the detection of low-concentration gas. The results showed that Cu₂O and Ga-ZnO formed an effective sensor array with an enhanced response of 8.5 to 5 ppm ethanol. Moreover, the CdO/LaFeO₃ and CdO/Sn-ZnO sensor array showed an enhanced response of 21 to 1 ppm ethanol and 14 to 1 ppm acetone with a low detection limit of <0.1 ppm. The high response of the sensor array is attributed to both the high response of the individual p- and n-type sensors and the multiplicity of the sensor array.

Author Contributions: J.L. synthesized the materials, carried out the characterizations, and wrote the draft; F.X. made the gas sensing measurements; X.Z. analyzed data; Z.X. built up the gas sensing measurement system and revised the manuscript; and Y.J. proposed the idea and revised the manuscript.

Conflicts of Interest: The authors declare no conflict of interest.

References

1. Yamazoe, N.; Shimano, K. New perspectives of gas sensor technology. *Sens. Actuators B Chem.* **2009**, *138*, 100–107. [[CrossRef](#)]
2. Yamazoe, N. Toward innovations of gas sensor technology. *Sens. Actuators B Chem.* **2005**, *108*, 2–14. [[CrossRef](#)]
3. Xiang, Q.; Meng, G.; Zhang, Y.; Xu, J.; Xu, P.; Pan, Q.; Yu, W. Ag nanoparticle embedded-ZnO nanorods synthesized via a photochemical method and its gas-sensing properties. *Sens. Actuators B Chem.* **2010**, *143*, 635–640. [[CrossRef](#)]
4. Korotcenkov, G. Gas response control through structural and chemical modification of metal oxide films: State of the art and approaches. *Sens. Actuators B Chem.* **2005**, *107*, 209–232. [[CrossRef](#)]
5. Han, N.; Tian, Y.J.; Wu, X.F.; Chen, Y.F. Improving humidity selectivity in formaldehyde gas sensing by a two-sensor array made of Ga-doped ZnO. *Sens. Actuators B Chem.* **2009**, *138*, 228–235. [[CrossRef](#)]
6. Liu, W.; Xu, L.; Sheng, K.; Zhou, X.; Dong, B.; Lu, G.; Song, H. A highly sensitive and moisture-resistant gas sensor for diabetes diagnosis with Pt@In₂O₃ nanowires and a molecular sieve for protection. *NPG Asia Mater.* **2018**, *10*, 293–308. [[CrossRef](#)]
7. Zhou, X.Y.; Wang, Y.; Wang, Z.; Yang, L.P.; Wu, X.F.; Han, N.; Chen, Y.F. Synergetic p plus n field-effect transistor circuits for ppb-level xylene detection. *IEEE Sens. J.* **2018**, *18*, 3875–3882. [[CrossRef](#)]
8. Korotcenkov, G.; Cho, B.K. Metal oxide composites in conductometric gas sensors: Achievements and challenges. *Sens. Actuators B Chem.* **2017**, *244*, 182–210. [[CrossRef](#)]
9. Xing, R.Q.; Xu, L.; Song, J.; Zhou, C.Y.; Li, Q.L.; Liu, D.L.; Song, H.W. Preparation and gas sensing properties of In₂O₃/Au nanorods for detection of volatile organic compounds in exhaled breath. *Sci. Rep.* **2015**, *5*, 10717. [[CrossRef](#)] [[PubMed](#)]

10. Kao, K.W.; Hsu, M.C.; Chang, Y.H.; Gwo, S.; Yeh, J.A. A sub-ppm acetone gas sensor for diabetes detection using 10 nm thick ultrathin InN FETs. *Sensors* **2012**, *12*, 7157–7168. [[CrossRef](#)] [[PubMed](#)]
11. Gu, H.S.; Wang, Z.; Hu, Y.M. Hydrogen gas sensors based on semiconductor oxide nanostructures. *Sensors* **2012**, *12*, 5517–5550. [[CrossRef](#)] [[PubMed](#)]
12. Pan, X.F.; Liu, X.; Bermak, A.; Fan, Z.Y. Self-gating effect induced large performance improvement of ZnO nanocomb gas sensors. *ACS Nano* **2013**, *7*, 9318–9324. [[CrossRef](#)] [[PubMed](#)]
13. Zhang, L.H.; Dong, B.; Xu, L.; Zhang, X.R.; Chen, J.J.; Sun, X.K.; Xu, H.W.; Zhang, T.X.; Bai, X.; Zhang, S.; et al. Three-dimensional ordered ZnO-Fe₃O₄ inverse opal gas sensor toward trace concentration acetone detection. *Sens. Actuators B Chem.* **2017**, *252*, 367–374. [[CrossRef](#)]
14. Shi, J.J.; Cheng, Z.X.; Gao, L.P.; Zhang, Y.; Xu, J.Q.; Zhao, H.B. Facile synthesis of reduced graphene oxide/hexagonal WO₃ nanosheets composites with enhanced H₂S sensing properties. *Sens. Actuators B Chem.* **2016**, *230*, 736–745. [[CrossRef](#)]
15. Xiang, Q.; Meng, G.F.; Zhao, H.B.; Zhang, Y.; Li, H.; Ma, W.J.; Xu, J.Q. Au nanoparticle modified WO₃ nanorods with their enhanced properties for photocatalysis and gas sensing. *J. Phys. Chem. C* **2010**, *114*, 2049–2055. [[CrossRef](#)]
16. Barsan, N.; Kozielj, D.; Weimar, U. Metal oxide-based gas sensor research: How to? *Sens. Actuators B Chem.* **2007**, *121*, 18–35. [[CrossRef](#)]
17. Han, N.; Wu, X.; Chai, L.; Liu, H.; Chen, Y. Counterintuitive sensing mechanism of ZnO nanoparticle based gas sensors. *Sens. Actuators B Chem.* **2010**, *150*, 230–238. [[CrossRef](#)]
18. Lee, J.H. Gas sensors using hierarchical and hollow oxide nanostructures: Overview. *Sens. Actuators B Chem.* **2009**, *140*, 319–336. [[CrossRef](#)]
19. Hu, P.; Yuan, F.L.; Bai, L.Y.; Li, J.L.; Chen, Y.F. Plasma synthesis of large quantities of zinc oxide nanorods. *J. Phys. Chem. C* **2007**, *111*, 194–200.
20. Chen, Y.J.; Zhu, C.L.; Wang, L.J.; Gao, P.; Cao, M.S.; Shi, X.L. Synthesis and enhanced ethanol sensing characteristics of alpha-Fe₂O₃/SnO₂ core-shell nanorods. *Nanotechnology* **2009**, *20*, 045502. [[CrossRef](#)] [[PubMed](#)]
21. Yude, W.; Xinghui, W.; Yanfeng, L.; Zhenlai, Z. The n + n combined structure gas sensor based on burnable gases. *Solid-State Electron.* **2001**, *45*, 1809–1813. [[CrossRef](#)]
22. Wang, Y.D.; Wu, X.H.; Zhou, Z.L. Novel high sensitivity and selectivity semiconductor gas sensor based on the p + n combined structure. *Solid State Electron.* **2000**, *44*, 1603–1607. [[CrossRef](#)]
23. Yang, L.F.; Wang, Y.L.; Wang, Y.D. Study on p + n combined structure semiconductor toluene gas sensing element. *Instr. Tech. Sens.* **2010**, *10*, 12–23.
24. Xie, Z.; Han, N.; Li, W.H.; Deng, Y.Z.; Gong, S.Y.; Wang, Y.; Wu, X.F.; Li, Y.X.; Chen, Y.F. Facet-dependent gas sensing properties of Cu₂O crystals. *Phys. Status Solidi A* **2017**, *214*, 1600904. [[CrossRef](#)]
25. Wang, J.X.; Yang, J.; Han, N.; Zhou, X.Y.; Gong, S.Y.; Yang, J.F.; Hu, P.; Chen, Y.F. Highly sensitive and selective ethanol and acetone gas sensors based on modified ZnO nanomaterials. *Mater. Des.* **2017**, *121*, 69–76. [[CrossRef](#)]
26. Parida, K.M.; Reddy, K.H.; Martha, S.; Das, D.P.; Biswal, N. Fabrication of nanocrystalline LaFeO₃: An efficient sol-gel auto-combustion assisted visible light responsive photocatalyst for water decomposition. *Int. J. Hydrog. Energy* **2010**, *35*, 12161–12168. [[CrossRef](#)]
27. Wang, Z.; Xie, Z.; Bian, L.; Li, W.; Zhou, X.; Wu, X.; Yang, Z.; Han, N.; Zhang, J.; Chen, Y. Enhanced NO₂ sensing property of ZnO by Ga doping and H₂ activation. *Phys. Status Solidi A* **2018**, *215*, 1700861. [[CrossRef](#)]
28. Han, N.; Chai, L.Y.; Wang, Q.; Tian, Y.J.; Deng, P.Y.; Chen, Y.F. Evaluating the doping effect of Fe, Ti and Sn on gas sensing property of ZnO. *Sens. Actuators B Chem.* **2010**, *147*, 525–530. [[CrossRef](#)]
29. Zhou, X.Y.; Wang, Y.; Wang, J.X.; Xie, Z.; Wu, X.F.; Han, N.; Chen, Y.F. Amplifying the signal of metal oxide gas sensors for low concentration gas detection. *IEEE Sens. J.* **2017**, *17*, 2841–2847. [[CrossRef](#)]
30. Zhang, Z.L.; Che, H.W.; Gao, J.J.; Wang, Y.L.; She, X.L.; Sun, J.; Gunawan, P.; Zhong, Z.Y.; Su, F.B. Shape-controlled synthesis of Cu₂O microparticles and their catalytic performances in the Rochow reaction. *Catal. Sci. Technol.* **2012**, *2*, 1207–1212. [[CrossRef](#)]
31. Bendavid, L.I.; Carter, E.A. First-principles predictions of the structure, stability, and photocatalytic potential of Cu₂O surfaces. *J. Phys. Chem. B* **2013**, *117*, 15750–15760. [[CrossRef](#)] [[PubMed](#)]

32. Tang, L.L.; Lv, J.; Sun, S.D.; Zhang, X.Z.; Kong, C.C.; Song, X.P.; Yang, Z.M. Facile hydroxyl-assisted synthesis of morphological Cu₂O architectures and their shape-dependent photocatalytic performances. *New J. Chem.* **2014**, *38*, 4656–4660. [[CrossRef](#)]
33. Guan, L.N.; Pang, H.A.; Wang, J.J.; Lu, Q.Y.; Yin, J.Z.; Gao, F. Fabrication of novel comb-like Cu₂O nanorod-based structures through an interface etching method and their application as ethanol sensors. *Chem. Commun.* **2010**, *46*, 7022–7024. [[CrossRef](#)] [[PubMed](#)]
34. Chen, T.; Zhou, Z.; Wang, Y. Effects of calcining temperature on the phase structure and the formaldehyde gas sensing properties of CdO-mixed In₂O₃. *Sens. Actuators B Chem.* **2008**, *135*, 219–223. [[CrossRef](#)]
35. Han, N.; Wu, X.; Zhang, D.; Shen, G.; Liu, H.; Chen, Y. CdO activated Sn-doped ZnO for highly sensitive, selective and stable formaldehyde sensor. *Sens. Actuators B Chem.* **2011**, *152*, 324–329. [[CrossRef](#)]



© 2018 by the authors. Licensee MDPI, Basel, Switzerland. This article is an open access article distributed under the terms and conditions of the Creative Commons Attribution (CC BY) license (<http://creativecommons.org/licenses/by/4.0/>).